Chapter 3
Broadband metamaterial absorber in the visible region using a petal-shaped resonator

We present an efficient broadband metamaterial (MTM) solar spectrum absorber with a wide incident angle and polarization-insensitive absorption. This is a three layers absorber in the form of a metal-dielectric-metal (resonator) structure. We use a single dielectric layer of silicon dioxide (SiO_2) between the metasurface (petal-shaped) and the lower layers of tungsten (W) metal. We obtained around 99% average absorption from 400 nm to 750 nm and a near-unity absorption at 572.23 nm wavelength. The unit cell structure shows 99% absorption from wavelengths from 456.62 nm to 677.73 nm and has an ultra-wide bandwidth (221.11 nm). For both the transverse magnetic (TM) and transverse electric (TE) modes, this design demonstrates wide-angle absorption up to 60^o. In addition, geometrical studies are carried out to obtain the optimized physical dimensions of the structure. We also analyze the weighted absorption under AM1.5 (air mass 1.5) solar luminosity by changing the thickness parameter of the SiO_2 layer. These properties can be used for thermophotovoltaics (STPV), solar cells, and energy harvesting devices.

3.1 Introduction

In the previous chapter, a logical mechanism was introduced for broadband metamaterial absorbers capable of showing somewhat broad absorption bandwidths. Photovoltaic cells are capable of converting light energy directly into electrical energy. So the lighter a photovoltaic cell absorbs, the more beneficial it is. In this chapter, a new metamaterial absorber design is introduced that completely covers visible wavelengths and shows nearly unity absolute absorption. Along with this, we have also investigated the absorption performance with different parameters, polarization angles, incident angles and others.

Solar cells are one of the most important and attractive devices in energy devices that play a vital role in providing pollution-free energy. Thinfilm solar cells have great advantages such as high flexibility, tunable properties, and low production cost [149,150]. Enhancing the efficiency of solar cells is the main issue. Many researchers have tried to solve this problem in different ways, such as using the light trapping method [151], grating [152], metallic nanoparticles [153], photonic crystals [154], and ultra-thin anti-reflection layer [155]. Our goal is to achieve higher conversion efficiency and to increase the short-circuit current density in the visible region.

Recently some researchers have been shown their interest in introducing a metamaterial (MM) absorber in solar cells [156,157]. That opens a new door for metamaterials (MMs) solar cell applications which solved problems such as absorption, wide incidence angle, efficiency, short-circuit current density, etc in solar cells [158]. The first metamaterial absorber was proposed by Landy et al.[72] and achieved around 88% absorption at 11.5 GHz due to the simultaneous excitation of magnetic and electrical resonances. The first THz metamaterial absorber was demonstrated by Tao et al. in 2008 [159] and reported about 70% absorption at 1.3 THz. Metamaterials exhibit an extraordinary property (negative permittivity and permittivity) with plasmonic resonance characteristics which is not

observed in conventional materials [6]. When an electromagnetic (EM) wave interacts with a metamaterial, it absorbs the EM waves, which can be used in a variety of devices [160]. If the metamaterial absorber structure absorbs all incident radiations, it is known as a perfect absorber. In this situation, the reflection, scattering, transmitting, and light propagation of the EM waves are negligible. To achieve perfect absorption, it is required to match the impedance of the metal with the free space impedance [161]. Broadband absorbers have been achieved above 80% [162] and more than 90% absorption [163–165]. To obtain the maximum absorption in the optical region, the metamaterial absorbers have been fabricated by the methods such as two-layer [166], three-layer [167], four-layer [92], and multi-layer [168], but the three-layered structures have been most commonly used. The three-layer (metal-dielectric-metal) based structure forms the coupling capacitance between the resonator and the bottom plane with the help of a spacer layer [169,170]. The metallic ground layer inhibits the propagation of electromagnetic waves resulting in near-zero transmission [171].

To obtain the perfect absorbance, many researchers have used gold (Au), silver (Ag), and aluminum (Al) metals, but these metals show poor thermal stability and the disadvantage of the single resonance frequency [172–174]. Researchers have been introduced new refractory metals such as chromium (Cr), tungsten (W), and nickel (Ni) that have high melting points and higher resonance frequencies [116,175,176]. These new plasmon metals are available at a low cost and are more suitable for producing the design of perfect broadband absorbers.

In this work, we have designed a new metamaterial absorber composed of three layers for the wavelength range from 400 to 750 nm. The proposed absorber exhibits around 98.96% average absorbance and wide absorption bandwidth from 456.62 nm to 677.73 nm. Tungsten (W) metal has a high melting point (3422 ºC) to tolerate high temperatures, and

also its impedance matching with free space is the main reason for choosing tungsten metal. The dielectric layer of silicon dioxide (SiO_2) also has high thermal stability (melting point at 1710 ºC) with lossless characteristics of low relative permittivity. This composition generates plasmonic resonance characteristics in the visible region with this geometrical structure [177–179]. We have studied the geometric parameters of the structure to obtain optimized absorbance. When the imaginary part of the impedance approaches zero and the real part of the impedance meets unity, we observe high absorption. A significant value of absorption $A_{AM1.5}$~99% and high conversion efficiency are achieved. We have also obtained the short circuit current density under AM1.5 for photovoltaic cells.

3.2 Design, simulation setup, and absorbance of the structure

3.2.1 Materials choice and structural parameters

The proposed absorber is composed of three layers with a petal-shaped (elliptical) tungsten (W) as a metasurface resonator, as shown in Fig. 3.1. A dielectric layer of silicon dioxide (SiO_2) is placed on top of the bottom layer of tungsten metal [140]. We have taken the thickness of the lower layer (h_m) to be 100 nm, and we obtain very small or almost zero transmission T(ω) due to the skin depth. The thickness of SiO_2 and the petal-shaped resonator are to be set as h_s = 60 nm and h = 60 nm, respectively. The period (p) of the unit cell is to be set as 300 nm in both the x and y directions. The petal-shaped structure has radii r_2 = 15 nm and r_1 = 110 nm. The top view of resonators and schematic diagram of the proposed absorber is shown in Fig. 3.1(a) and 3.1(b). The main reasons for choosing tungsten as a metal layer and Patel shape resonator because of its high impedance and high intrinsic losses. High intrinsic losses cause the transmission through the ground slab to be almost zero and reduce the reflection throughout the unit cells. High intrinsic losses also help in broadband absorption for tungsten naturally in the visible region by a good impedance matching with the free space by the proposed absorber structure. Tungsten itself

is also an excellent absorber on its own with a low ohmic loss. The lossless characteristics of SiO_2 give us the intention to choose it as the dielectric spacer. Its resonance characteristics also help the design to impedance match. Hence, this high absorbance of the proposed (tungsten-based) design is solely achieved due to its impedance matching with free space.

3.2.2 Simulation setup

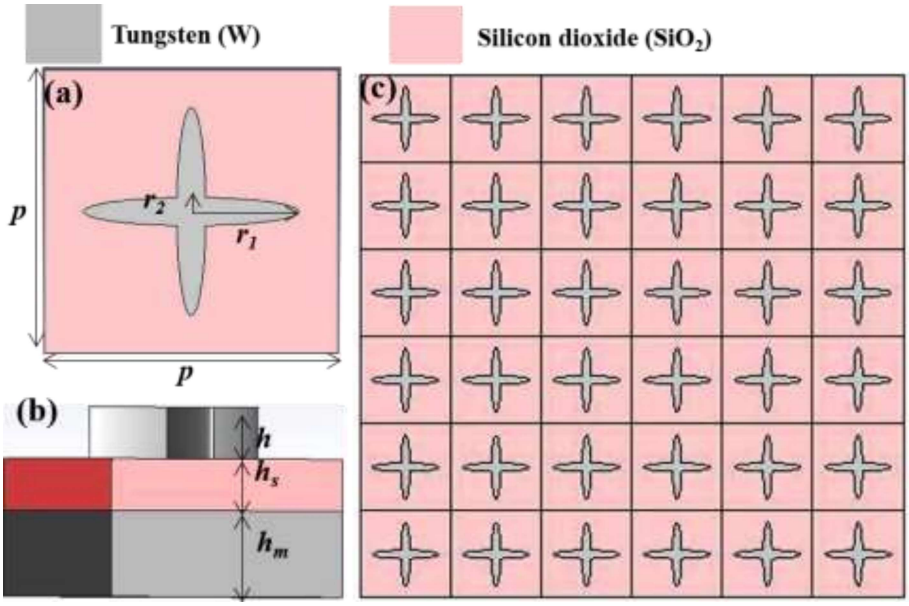

Fig. 3.1 Geometry design of the proposed metamaterial absorber, **(a)** front-view of the unit cell, **(b)** schematic view of the absorber, **(c)** unit cells in a periodic arrangement.

Fig. 3.1(a) shows the petal-shaped metasurface of the metamaterial absorber, and Fig. 3.1(b) represents the structural geometry of the proposed design. Fig. 3.1(c) demonstrates the periodic unit cells. We apply the periodic boundary conditions (PBCs) in the x and y-direction, and the electromagnetic (EM) waves propagate along the z-direction (open space). All the data is taken from the CST software, which is based on the theory of finite integration technique (FIT) [180]. The effects of different parameters on the absorbance and the absorber are discussed later.

3.2.3 The Absorbance of a unit cell

The reflectance should be minimum to design a perfect broadband metamaterial (MM) absorber. The absorption of the unit cell is obtained by the formula [171] given by,

$$A(\omega) = 1 - T(\omega) - R(\omega) \tag{3.1}$$

Where, $A(\omega)$, $T(\omega)$, and $R(\omega)$ are frequency-dependent absorbance, transmission, and reflectance parameters, respectively. If the thickness of the bottom plane is more than the skin depth, tungsten blocks the maximum transmittance, so $T(\omega)$ will be zero and the absorption can be obtained by this formula,

$$A(\omega) = 1 - R(\omega) = 1 - |S_{11}|^2 \tag{3.2}$$

Where S_{11} represents the scattering parameter.

The reflection and absorbance of a unit cell are shown in Fig. 3.2. Where reflection is minimum and absorption is maximum in the obtained spectrum. The proposed absorber has a 99.99% absorbance at a 572.23 nm wavelength. It shows over 99% absorption from 456.62 nm to 677.73 and covers a wide bandwidth (221.11 nm). The average absorbance of the structure is 98% for the whole visible region. Fig. 3.3(a) exhibits a critical impedance matching condition for nearly perfect absorption. If the imaginary part of the impedance is reached near zero and the real part of the impedance goes nearly the unity, it will make a perfect metamaterial absorber. Tungsten metal has shown excellent impedance with free space. Since W metal does not support the surface plasmons in the optical region, high absorbance is ascribed to match the condition of impedance with free space and showed as perfect absorbance. The resonance characteristics of SiO_2 and the intrinsic loss of resonators also help to gain excellent impedance. The fabrication process of the proposed absorber has serval simple steps such as spin coating, electron beam printing for tungsten metasurface, evaporation, and lift-off phase [181].

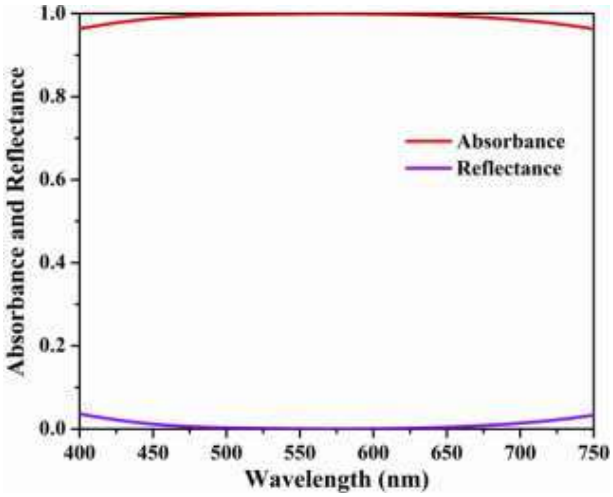

Fig. 3.2 Absorbance and reflectance of the proposed absorber.

3.2.4 Extraction of S-parameters

One of the methods to estimate the maximum absorbance is impedance matching. When the impedance of tungsten z_{eff} matches with free space impedance z_0=1, absorbance will be maximum. We have investigated the relationship between scattering parameters and impedance to understand the behavior of absorbance. The *s*-matrix elements are given as follows [182],

$$S_{11} = \frac{\left(\frac{z_{eff}-1}{z_{eff}+1}\right)\left(1-e^{i2kdn_{eff}}\right)}{1-\left(\frac{z_{eff}-1}{z_{eff}+1}\right)^2 e^{i2kdn_{eff}}} \tag{3.3}$$

$$S_{21} = \frac{\left(1-\left(\frac{z_{eff}-1}{z_{eff}+1}\right)^2\right)e^{i2kdn_{eff}}}{1-\left(\frac{z_{eff}-1}{z_{eff}+1}\right)^2 e^{i2kdn_{eff}}} \tag{3.4}$$

Where S_{11} and S_{21} are scattering parameters of the matrix, d is the maximum length of the structure, k is the wave vector, and n_{eff} is the refractive index. The magnitude and phase of s-parameters are extracted based on the dominant modes responsible for the transfer of power in significant forms. Fig. 3.3(a) and 3.3(b) show the magnitude and phase of S_{11} and S_{21} parameters, respectively. Utilized the s-parameters, other parameters such as refractive index, effective impedance (z_{eff}), effective permittivity (ε_{eff}), and effective permeability

(μ_{eff}) of the device can be calculated by giving these formulas at the normal incidence angle. So, the impedance can be calculated by [183],

$$z_{eff} = \pm\sqrt{\frac{(1+S_{11})^2 - S_{21}^2}{(1-S_{11})^2 - S_{21}^2}} = \frac{1+S_{11}}{1-S_{11}} \tag{3.5}$$

$$e^{inkd} = \frac{S_{21}}{1-\left(\frac{z_{eff}-1}{z_{eff}+1}\right)S_{11}} \tag{3.6}$$

$$n_{eff} = \frac{1}{kd}\left[\{[\ln(e^{inkd})]'' + 2m\pi\} - i[\ln(e^{inkd})]'\right] \tag{3.7}$$

$$\varepsilon_{eff} = \frac{n_{eff}}{z_{eff}};\ \mu_{eff} = n_{eff}\, z_{eff} \tag{3.8}$$

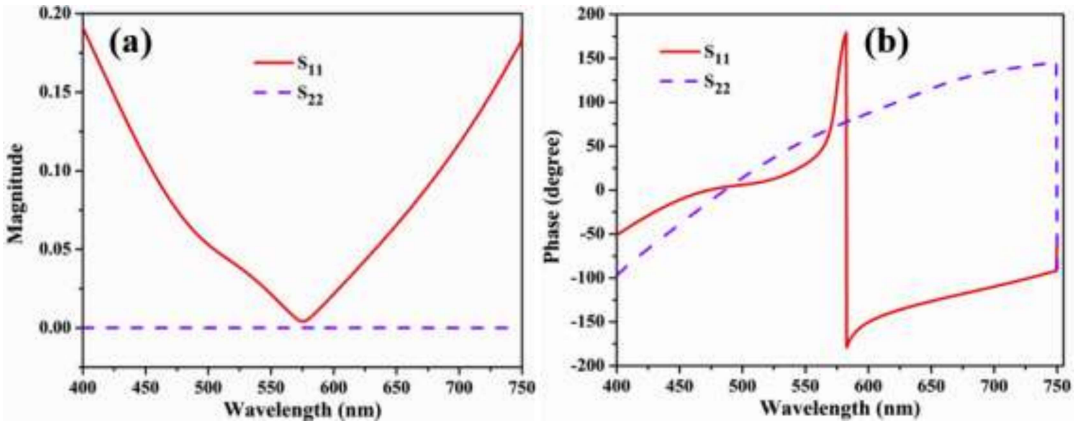

Fig. 3.3 (a) Magnitude of *S*-parameters, **(b)** phase (degree) of *S*-parameters of proposed absorber obtained from *CST-MSW*.

Fig. 3.4(a) and 3.4(b) show the effective impedance (z_{eff}) and refractive index (n_{eff}). Fig. 3.4(c) and 3.4(d) show the imaginary and real parts of effective permittivity and permeability, respectively. The real part of electrical permittivity must be equal to the magnetic permeability, and the imaginary part of these effective parameters should dissipate the maximum energy of electromagnetic waves for the perfect absorber. The electric field distribution is the main reason for the resonant wavelength variation.

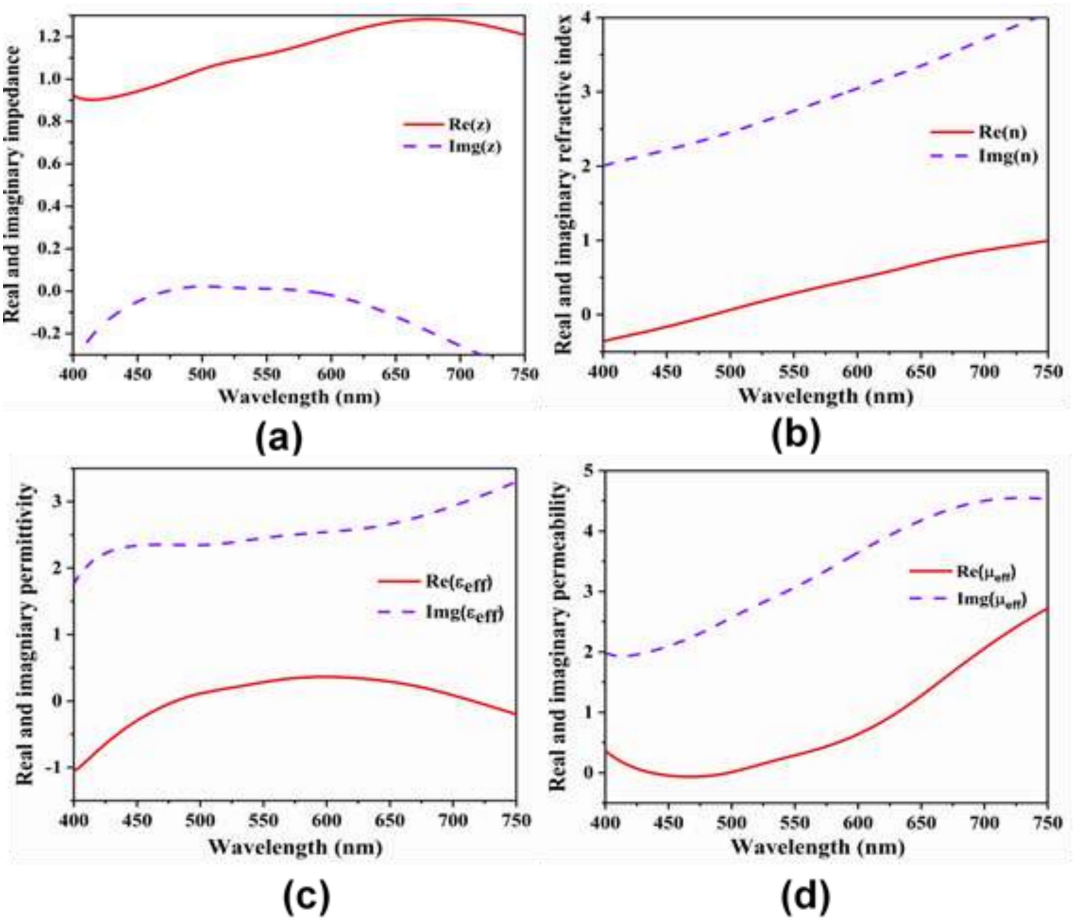

Fig. 3.4 (a) Real and imaginary parts of normalized impedance, **(b)** refractive index, **(c)** permittivity, and **(d)** permeability, respectively.

3.3 Result and discussion

3.3.1 Effect of the thickness of resonators

First, we investigate the absorbance performance of the metasurface thickness (h). We only change the thickness of the petal-shaped resonator (h) here, and other parameters are kept unchanged. Fig. 3.5 exhibits the absorbance spectra for various thickness values of the metasurface. The thickness varies from 40 nm to 80 nm with a 10 nm interval. When the thickness of the resonator is 60 nm, we observe wider absorbance bandwidth and show the near-unity perfect absorbance. The average absorption is gained at around 98.96% in the whole visible region. By decreasing and increasing the thickness of resonators, the average

absorption changes with the absorption spectra. The average absorption is 97.76%, 98.67%, 98.96%, 98.78%, and 98.36% for 40 nm, 50 nm, 60 nm, 70 nm and 80 nm, respectively.

Here, optical impedance plays a crucial role in the performance of the MM absorber. We have calculated the impedance of the absorber with the help of scattering parameters which shows the real and imaginary parts of the normalized impedance for h = 60 nm. When the real part of the impedance equals the impedance of air, the reflectance becomes minimum and exhibits perfect absorption. It is the main reason for gaining high absorption in the whole region.

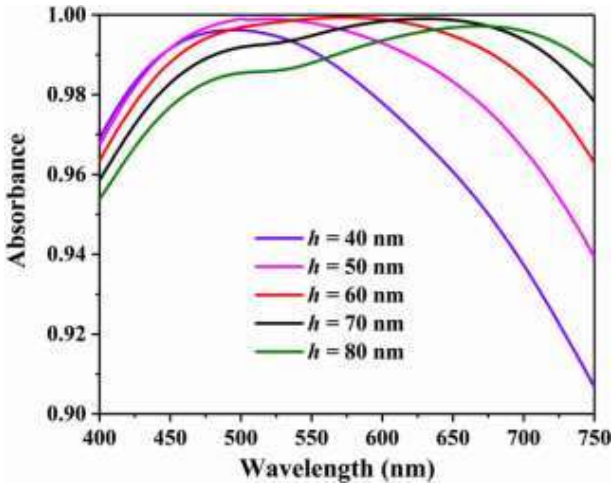

Fig. 3.5 The absorbance performance with the different thicknesses (h) of the petal-shaped resonator.

3.3.2 Effect of the semi-major and semi-minor axis of the petal-shaped resonator

We also investigate the effect of absorbance performance with a radius of resonators and fixed other absorber parameters. The optimum radius of the resonator considers being as r_1 = 110 nm. Fig. 3.6(a) demonstrates the absorption spectra with the different semi-major axis (r_1) and shows the over 98.96% average absorption from 400 nm to 750 nm. By decreasing and increasing r_1 from 90 nm to 130 nm with 10 nm intervals, the absorption spectra change due to magnetic resonance between the petal-shaped resonators and the ground plane of the substrate [184,185].

To get a better performance of the absorber, we change the semi-minor axis (r_2) of the petal-shaped resonator, as shown in Fig. 3.6(b). The semi-minor axis varies from 5 nm to 25 nm with 5 nm intervals. The optimum semi-minor axis is 15 nm which exhibits a near-unity absorption. When the semi-minor axis changes, the absorption curves shift and decrease the average absorption. Therefore, the geometrical parameters of the resonator play a crucial role in achieving perfect absorption.

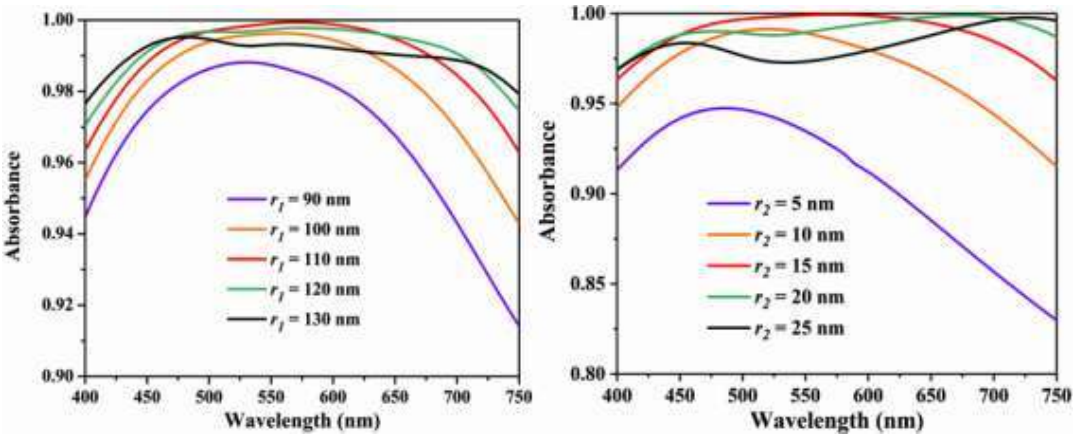

Fig. 3.6 Spectrum performance with **(a)** the different semi-major axis, **(b)** the different semi-minor axis.

3.3.3 Effect of the thickness of the dielectric layer

A significant variation is found at the sweep of a dielectric thickness (h_s) and exhibited in Fig. 3.7. After changing the thickness of the dielectric layer from 40 nm to 80 nm with a step of 10 nm, we observed a significant change in absorbance. The proposed absorber shows different average absorption for different dielectric thicknesses. For the different thicknesses of the dielectric of 40 nm, 50 nm, 60 nm, 70 nm, and 80 nm, we obtain different average absorbances of 95.74%, 98.68%, 98.96%, 96.13%, and 90.59%, respectively. The change in the resonator capacitance causes the optical spectra changes. The capacitance value is inversely proportional to the intermediate plane of the thickness. When the resonant frequency increases, the capacitance decreases. The capacitance and

inductance are responsible for shifting the resonance wavelength as the changes in dielectric layer thickness. With this phenomenon, the proposed unit cell may be used to detect the thickness of any semiconductor layer or optical sensor.

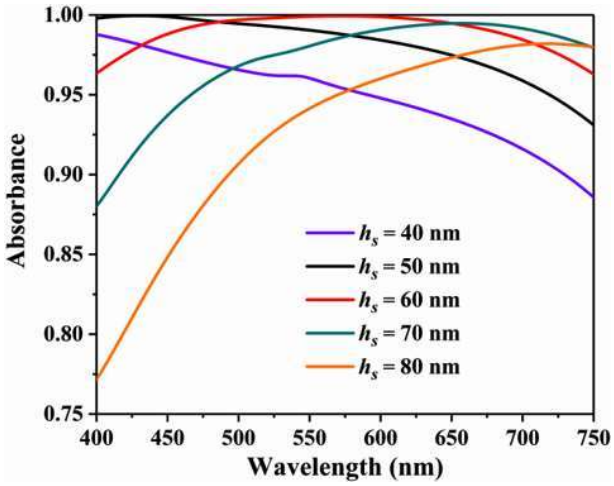

Fig. 3.7 Spectrum performance with different thicknesses of the dielectric layer.

3.3.4 Polarization and incident angle independency

For the ideal case, the absorber must be independent of polarization and incident angle of light to use as a solar sensor or detector, solar energy harvesting, solar cell, and other optical applications. At normal incidence, we have investigated the impact of different polarization directions on absorption performance. The polarization direction along the x-direction (TE polarization) is indicated by a polarization angle of zero, while the polarization direction along the y-direction (TM polarization) is indicated by a polarization angle of 90. The absorption spectrum of the perfect absorber is illustrated in Fig. 3.8. As the polarization direction changes, the absorption spectra of the perfect absorber remain constant. It's because of the petal-shaped resonator's geometric symmetry. The absorption of the absorber is stable when it is polarization-independent.

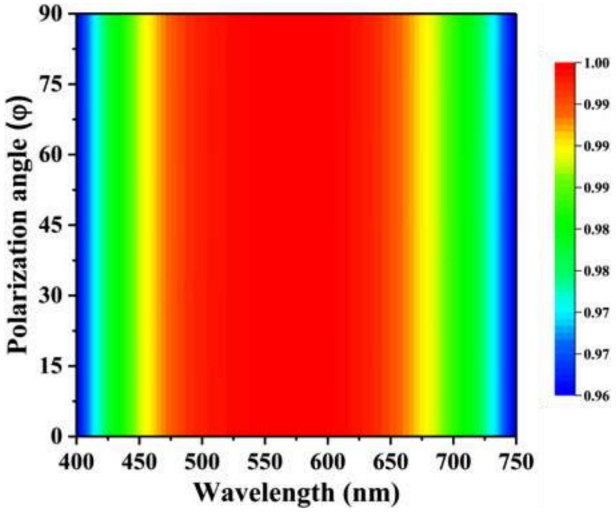

Fig. 3.8 Absorbance spectra with different polarization angles (φ) from 0º to 90º

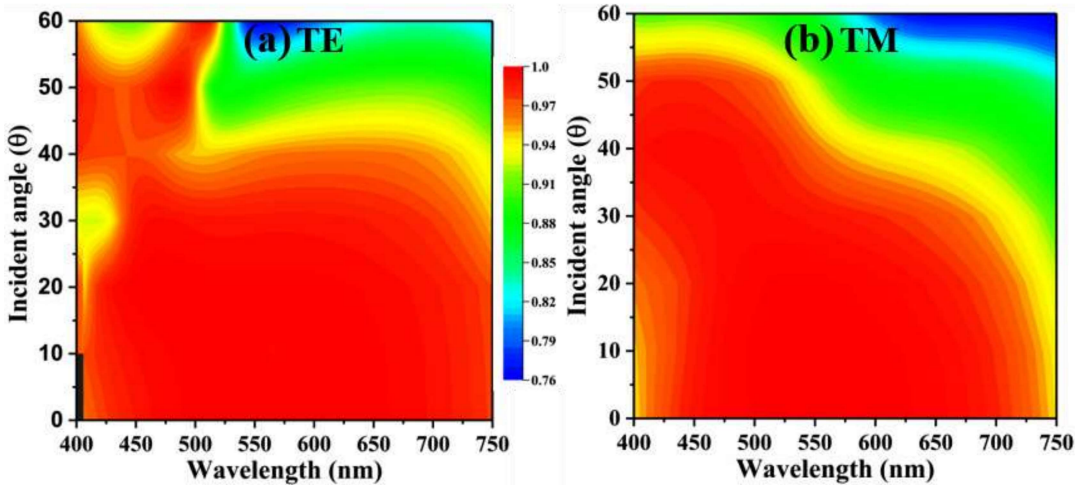

Fig. 3.9 Absorbance spectra with different incident angles (θ) from 0º to 60º, **(a)** for TE mode, **(b)** for TM mode.

Fig. 3.9(a) and 3.9(b) reveal the absorption spectra at different incident angles for both TE and TM modes, respectively. We obtain the average absorption of 96.00% and 96.84 for all TE and TM mode incident angles, respectively. The absorber shows similar absorption behavior at a normal incident angle due to the symmetric geometry for both modes. By increasing the incident angle, absorption decreases for both modes due to the confinement of a weak electromagnetic field in the dielectric medium. In other words, we can say that absorption decreases when the angle of incidence is increased from minimum

to maximum and peak absorption decreases as the resonance wavelength increases. This is because the larger the angle of incidence, the longer the path length and the smaller the coupling effect. The electromagnetic dipole resonance is reduced due to the reduced coupling effect, resulting in less wave binding in the dielectric layer. Nonetheless, with a varied incident angle, the proposed absorber has a competitive appearance. As a result, the suggested absorber is an excellent option for an incidence angle stability-based metamaterial absorber that is polarisation insensitive.

3.3.5 Absorbance comparison with various spacer planes and metals

Here we check the absorbance performance of different dielectric materials and metals. Fig. 3.10(a) and 3.10(b) show low- and high-level optical spectra. First of all, we replace the dielectric layer of silicon oxide with other dielectric materials to show the absorption in Fig. 3.10(a). Here, silicon dioxide (SiO_2), silicon nitride (Si_3N_4), silicon amorphous (A-Si), and gallium arsenide (GaAs) have refractive indexes of 1.5, 2.0, 4.4, and 3.9, respectively. The change in refractive index causes the absorption level in each material to change. As is well known, the lower the refractive index, the higher the absorption and the higher the bandwidth. As can be seen, SiO_2 produced the best results since it has the lowest refractive index of all the materials.

Finally, we compare the absorption performance in the optical field by alternating the design metal with other different metals, as shown in Fig. 3.10(b). Absorbance is investigated by replacing tungsten (W) metal with aluminum (Al), silver (Ag), nickel (Ni), and chromium (Cr) metals, respectively. Excellent impedance matching condition with free space in the complete optical region makes it a perfect absorber. Here, Al, Ag, Ni, and Cr materials indicate the average absorbance levels of 66.95%, 64.55%, 90.96%, and 78.44%, respectively. Al and Ag do not exhibit better absorption because they do not match the

desired impedance with the design of this structure. As a result, the suggested (tungsten-based metal) design's high absorbance is exclusively owing to its impedance matching with free space, as evidenced by the front layer's resonance and rear layer intrinsic loss.

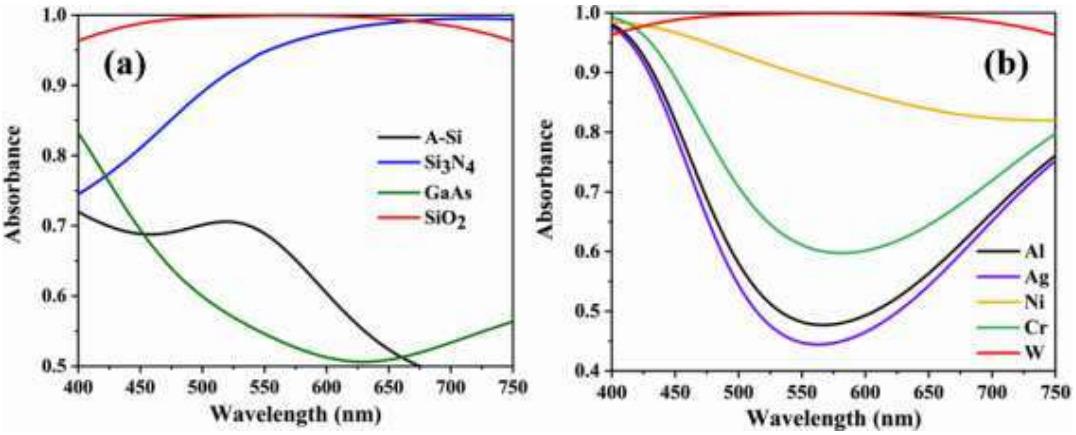

Fig. 3.10 (a) Absorbance spectra with a different dielectric material, **(b)** Absorbance spectra with the different metal of petal-shaped resonator.

3.3.6 Conversion efficiency $A_{AM1.5}$ (%)

Different structures of absorbers exhibit various significant absorption under the AM1.5 solar spectrum. Fig. 3.11 shows the large value of $A_{AM1.5}$ around 99% and reveals the high conversion efficiency at an optimum thickness (h = 60 nm) of the dielectric layer. The light-tapping effect of a unit cell proves wrong this assumption that collection efficiency and carrier transport are constant in the solar cell.

The value of $A_{AM1.5}$ can be calculated by this formula [143],

$$A_{AM1.5} = \frac{\int_{\lambda_{min}}^{\lambda_{max}} A(\lambda)\, G(\lambda)\, d\lambda}{\int_{\lambda_{min}}^{\lambda_{max}} G(\lambda)\, d\lambda} \tag{3.9}$$

Where λ_{max} and λ_{min} are the wavelength of light and define the absorption spectrum range under the AM1.5 solar illumination. Here, $A(\lambda)$ and $G(\lambda)$ represents the absorption of light and the distribution of photon numbers. Table 3.1 represent all values of absorption $A_{AM1.5}$ (%) with different thickness of the SiO_2 layer.

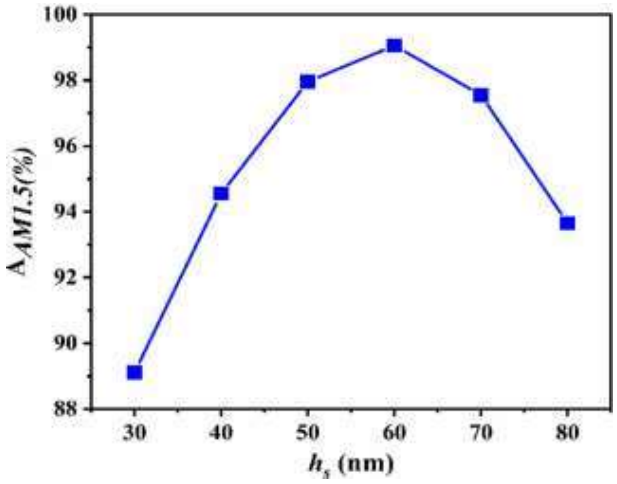

Fig. 3.11 Solar conversion efficiency ($A_{AM1.5\ (\%)}$) versus different thicknesses (h_s) of a silicon-dioxide layer.

Table 3.1 $A_{AM1.5}$with different thicknesses (h_s) of SiO_2 layer.

Thickness (h_s)	**30 nm**	**40 nm**	**50 nm**	**60 nm**	**70 nm**	**80 nm**
$A_{AM1.5}$(%)	89.12 %	94.55%	97.96%	99.06%	97.55%	93.65%

3.3.7 Short-circuit current density (J_{sc}), Solar spectrum and Efficiency of solar cells

For solar cell applications, it is very important to have the highly desired broadband absorption in the absorbing layer. To obtain the photophysical performance of this absorber need to short circuit current density (J_{sc}) and calculated by the given formula under the AM1.5G solar illumination [148].

$$J_{sc} = \frac{e}{hc}\int_{\lambda_{min}}^{\lambda_{max}} \lambda\, \Phi_{AM1.5}(\lambda)\, A(\lambda)\, d\lambda \tag{3.10}$$

Where e is the charge of the electron, c is the speed of light, h is Plank's constant, λ is the wavelength of light, $A(\lambda)$ is the absorption of the absorber, $\Phi_{AM1.5}(\lambda)$ is the solar radiance AM1.5(global tilt). The intrinsic quantum efficiency is assumed to be 100%. Fig. 3.12(a) shows the influence of short circuit density on different thicknesses of the SiO_2 layer and

mentions all J_{sc} values in Table 3.2. We obtained the high value of (J_{sc}~26.41 mA/cm^2) at optimum thickness (h = 60 nm) which is much larger than 17.08mA/cm^2 [172].

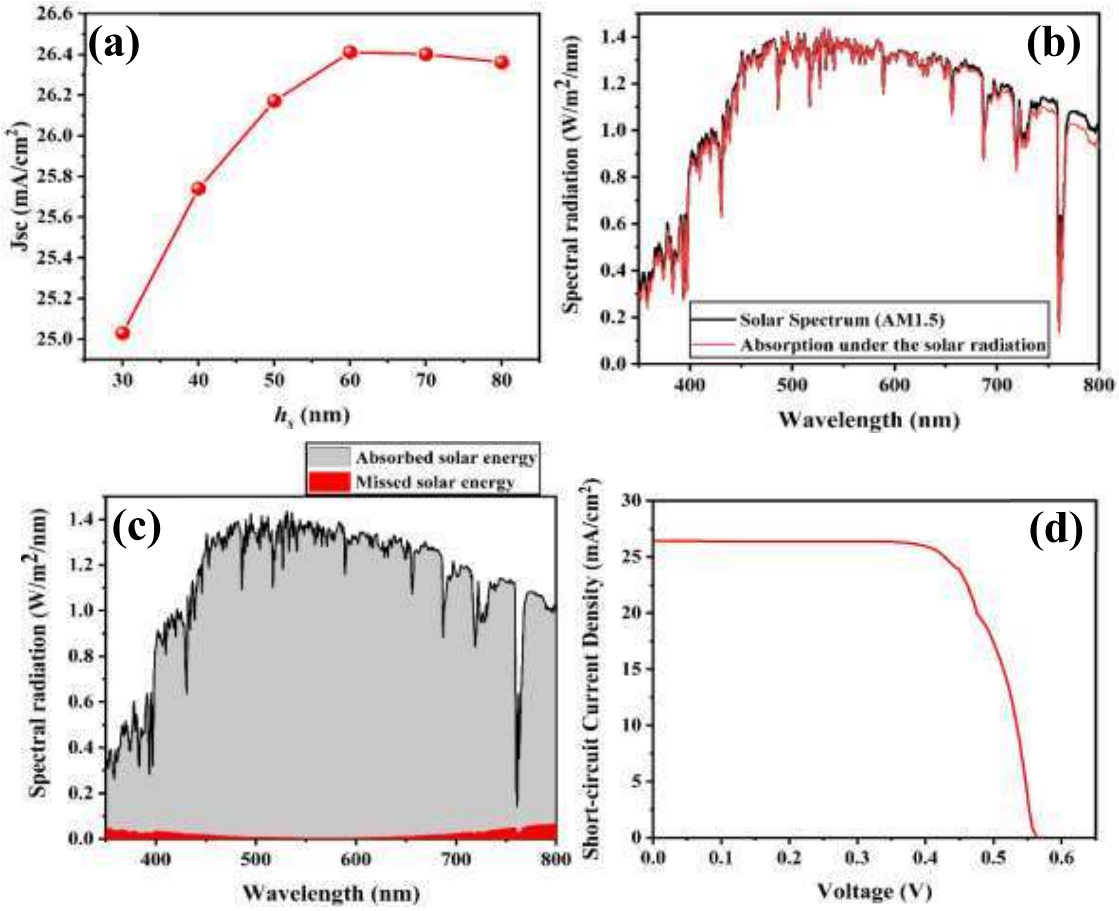

Fig. 3.12 (a) Short circuit current density with different thicknesses (h_s) of silicon dioxide layer, **(b)** Absorption under the solar radiation, **(c)** Absorb energy and the missed solar energy under the AM1.5(Air Mass 1.5), and **(d)** *J-V* curve of the proposed metamaterial solar cells.

Table 3.2 Shows all values of J_{sc} with the changed thickness of the SiO_2 layer.

Thickness (h_s)	**30 nm**	**40 nm**	**50 nm**	**60 nm**	**70 nm**	**80 nm**
J_{sc}(mA/cm^2)	25.04	25.74	26.17	26.41	26.39	26.36

The study of solar energy collection is usually used to understand solar absorption responses. The ideal absorber possesses broadband absorption with a wide bandwidth

range. We investigate the absorption under AM1.5 solar radiation. Fig. 3.12(b) shows the absorption under solar radiation and the AM1.5 solar spectrum. Fig. 3.12(c) shows the absorbed solar energy and the missed solar energy of the presented absorber. Multiple resonance coupling in the wide wavelength range is responsible for gaining broad absorption near unity. Therefore, this proposed absorber can significantly contribute to capturing potential applications such as solar energy harvesting and ultra-thin solar cells.

As shown in Fig. 3.12(a), we have already calculated the short circuit density (J_{sc}) for different thicknesses of silicon dioxide. At 60 nm thickness of SiO_2, we have obtained the highest J_{sc} value which is 26.41 mA/cm^2. In this section, we have theoretically calculated the open-circuit voltage (V_{oc}), fill factor, and efficacy of the proposed metamaterial solar cells. The open-circuit voltage can be calculated by the given equation [186],

$$V_{oc} = \frac{K_B T}{e} ln \left[\frac{J_{sc}}{J_0} + 1\right] \tag{3.11}$$

Where, K_B, h, e, and T represent the Boltzmann constant, Plank's constant, the charge of an electron, and room temperature (300K). J_{sc} is the short circuit current density and J_o is the saturation current which can be calculated as,

$$J_o = -2\pi e \int_0^{\lambda_g} \frac{2hc^2}{\lambda^5} \frac{1}{\left[exp\left(\frac{1}{K_B T} \times \frac{hc}{\lambda}\right) - 1\right]} d\lambda \tag{3.12}$$

Conversion efficiency is the percentage of solar energy shining on the solar cell's photovoltaic cell device that is converted into usable electricity. The efficiency (η) of designed metamaterial solar cells can be theoretically calculated using the below equation,

$$\eta = \frac{FF \times V_{oc} \times J_{sc}}{P_{in}} \tag{3.13}$$

where P_{in} is the incident flux at solar spectrum A.M 1.5 is 1000 W/m^2.

Therefore, using these above equations, we have obtained the values of V_{oc}, FF, and η which are 0.56V, 81.79%, and 12.09%, respectively. Fig. 3.12(d) shows the *J-V* curve of the proposed MTM solar cells.

3.3.8 Comparative study

The proposed absorber covers the entire optical region. Here, we have compared the different types of metamaterial absorbers with different layers arrangement in the optical wavelength region. Table 3.3 is listed details of compared absorbers. We have observed a good absorbance in this chapter by taking three layers that show excellent average absorption (98.96%) compared to others. This structure is designed by keeping in mind the cost-effective materials used and high-temperature stability compared to other structures. The operating of an incident angle up to 60° plays a crucial role in solar cell and solar energy harvesting applications. Therefore, all these reasons make the proposed design sufficient for potential solar energy harvesting applications in the visible region.

Table 3.3 Comparison study of the proposed absorber with various previous works.

Range (nm)	**Dimensions (nm)**	**Number of layers**	**Materials used**	**Absorption (%)**	**Angular stability (θ ≥70°)**	**Polariza-tion in sensitive**	**Ref.#**
262-709	240×240×170	Two	Au, Si	Above 90%	θ ≤50°	Yes	166
400-800	300×300×240	Three	TiN, SiO_2	Above 87%	θ ≤ 50°	Yes	167
575-750	500×500×240	Four	Ai, Kerr	Above 80%	θ ≤ 40°	Yes	92
430-850	320×320×50	Three	Au, SiO_2	Above 90%	θ ≤ 40°	Yes	169
400-850	500×500×174	Three	Al, SiO_2	N/A	N/A	No	170
400-750	300×300×220	Three	W, SiO_2	Above 98%	θ ≤ 60°	Yes	**This work**

3.4 Conclusion

We have proposed a polarization-insensitive, broadband, and wide-angle-based metamaterial absorber for a 400 to 750 nm wavelength range with an average of 98.96% absorbance. We have used silicon dioxide semiconductors with a low refractive index (1.5) and tungsten metal with a high melting point (3422 ºC). The proposed absorber shows suitable impedance, which matches the impedance of free space, and exhibits a perfect absorption over the entire applied area. We have derived the effective parameters of the metamaterial with the help of scattering parameters and phases. We have also studied the geometric parameters of the proposed unit cell, such as the dielectric thickness and the resonator's thickness along the semi-major and semi-minor axis. The proposed absorber exhibits a wide bandwidth with different incident angles (0º–60º) for TE and TM modes. Under solar illumination AM1.5, we have obtained significant absorption performance $A_{AM1.5}$~99% and short circuit current density (J_{sc} = 26.41 mA/cm^2). These characteristics of the proposed absorber make it an ideal candidate for solar cell applications. In addition, we have also calculated the open-circuit voltage (0.56V), fill factor (81.79%), and efficiency (12.09%) for the metamaterial solar cells in this study.